Journal of Environmental Management 370 (2024) 122574

Contents lists available at ScienceDirect

Journal of Environmental Management

journal homepage: www.elsevier.com/locate/jenvman

Research article

Atmospheric pressure dielectric barrier discharge plasma for in-situ water treatment using a bubbling reactor

Xin Tang [a,*], Antônio D.N. Ferraz Júnior [b], Kersti Karu [c], Luiza C. Campos [b], Minkwan Kim [a,**]

[a] Department of Aeronautics and Astronautics Engineering, University of Southampton, SO16 7QF, United Kingdom
[b] Centre for Urban Sustainability and Resilience, Department of Civil, Environmental and Geomatic Engineering, University College London, Gower Street, London, WC1E 6BT, United Kingdom
[c] UCL Chemistry Mass Spectrometry Facility, Department of Chemistry, University College London, London, WC1E 6BT, United Kingdom

ARTICLE INFO

Keywords:
In-situ resource utilization (ISRU)
Non-thermal plasma
Dielectric barrier discharge
Sulfamethoxazole degradation
E. coli K12 inactivation

ABSTRACT

Non-thermal plasma has been an emerging technology for water treatment for decades. In this study, we have designed and fabricated a bubbling plasma batch reactor using an atmospheric pressure dielectric barrier discharge with a hydrophobic porous membrane. The reactor performance is assessed for purifying synthetic contaminated water samples containing chemical contaminant sulfamethoxazole (SMX), a widely used antibiotic, and biological contaminant *E. coli* K12. The SMX decontamination tests indicate that the degradation process is not first-order and the reaction rate dwindle with increasing initial concentration. The yield at 50% removal achieves its highest value of 8.12 g/kWh for 50 mg/L SMX sample. For inactivation of *E. coli* K12 tests, the inactivation process is also not first-order, and the pathogen is completely inactivated for 10^2 CFU/mL and 10^4 CFU/mL cases after 10 min and 45 min of plasma treatment, respectively. For the 10^8 CFU/mL sample, a 5-log reduction is achieved after 60 min of treatment. The developed plasma reactor can achieve fast deployment in point of use, low cost for manufacturing, and simple for maintenance. Moreover, it can be used for in-situ water purification in future long duration crewed space missions as well as tackling with water pollution issues on our planet.

1. Introduction

Conventional water treatment technologies have limited efficiency for the removal of certain pollutants, such as pharmaceuticals (Magureanu et al., 2021), perfluoroalkyl substances (PFAS) (Stratton et al., 2017; Trojanowicz et al., 2018), and endocrine disrupting compounds (Benotti et al., 2009). The increasing number of antibiotics are of great concern due to their toxicity and potential to induce resistance in drugs acting on aquatic ecosystems and human health (Marx et al., 2015). The conventional biological process is ineffective in removing antibiotics, which can lead to adverse effects on ecological balance and public health. This may be due to the fact that the design objective of antibiotics is to sterilize bacteria (Lucas et al., 2016).

As one of the most widely used sulfonamide antibiotics, sulfamethoxazole (SMX) is frequently detected in the aquatic environment (Al Aukidy et al., 2012). Its interference with folate production in bacteria (Bilea et al., 2024), and disruption of the folate biosynthetic pathway (Brain et al., 2008) affects virtually every process in plants (Gorelova et al., 2017). These challenges prompt a search for more efficient and more cost-effective methods for water treatment. Non-thermal plasma is a novel technology to complement or replace classic methods for water decontamination, purification, and disinfection (Foster, 2017; Jiang et al., 2014; Magureanu et al., 2021; Zeghioud et al., 2020). Reactive species (reactive oxygen species, ROS: •OH, O, H_2O_2, O_3 etc.; and reactive nitrogen species, RNS: NO, NO_2, NO_3, HONO, HNO_2, NH etc.) are generated during atmospheric pressure plasma water treatment (Bradu et al., 2020; Brisset and Pawlat, 2016; Jiang et al., 2014; Samukawa et al., 2012). Atmospheric pressure air DBD is extensively investigated as one of the non-thermal plasma discharge for water treatment due to its easy manufacturing, simple electrode structure, and operating gas condition (Tang et al., 2018).

For manned space flight, water is one of the key technical challenges in long duration space missions since potable water is essential to sustain the life of astronauts. In-situ resource utilization (ISRU) and the recycle/

* Corresponding author.
** Corresponding author.
E-mail addresses: x.tang@soton.ac.uk, jamestangx@gmail.com (X. Tang).

https://doi.org/10.1016/j.jenvman.2024.122574
Received 12 June 2024; Received in revised form 12 September 2024; Accepted 16 September 2024
Available online 24 September 2024

reuse of on-board water are the only practical options for surface expeditionary crews and future par-point outposts. Minimizing the amount of water carried from Earth will enable the affordable establishment of extra-terrestrial exploration and operations since more equipment can be carried to help enable new scientific discoveries. The International Space Station (ISS) onboard medical kit for crew members contains a substantial number of antibiotics formulated for topical and systemic use. These antibiotics can be present in the final treated drinking water of modern water treatment facilities (Boleda et al., 2014), potentially becoming chemical contaminants in water treatment system within the spacecraft or space station, which may affect the susceptibility of microorganisms (Taylor, 2015). Biological contaminants can remain in the purified water in the current water recovery and management system of the ISS (Thompson et al., 2020). These bacteria can group together and coat the sides of the water pipes, forming biofilm. Biofilm may lead to life-threatening infections in astronauts (Singh et al., 2018) and can also clog the spacecraft's water pipes (Diaz et al., 2019; Zea et al., 2018), posing a demanding challenge for astronauts to fix. As summarized in a comprehensive review, plasma-based water treatment technology could be potentially modularized and scaled-up for in-situ water resource utilization or point of use applications in regions lacking water treatment infrastructure as well as integrated with conventional water treatment systems (Foster, 2017). Non-thermal plasma water treatment technology exhibits considerable potential for addressing the challenges of treating chemically and biologically contaminated water in space applications.

In this paper, our aim is to design and fabricate a proof-of-concept portable plasma water batch reactor using a flexible dielectric barrier discharge (DBD) with air at atmospheric pressure to tackle the aforementioned challenges. It is easy to assemble for fast deployment in point of use situations, low cost for manufacturing, and simple for maintenance. The flexible DBD exhibits greater versatility compared to rigid-structure DBD and can be applied to a broader range of targets including wound treatment on the human body, public surface disinfection, or food sterilization (Nguyen et al., 2024). The compactness and flexibility of the surface DBD (Allabakshi et al., 2022) make it possible to place the plasma source close to the bottom of treated water separated by a thin hydrophobic membrane. Air flow is introduced through the porous holes in the surface DBD, carrying reactive species and entering the target solution instantly via bubbling. Since the electrodes are not in contact with the treated water directly, the conductivity of the water will not affect the discharge state. This configuration overcomes practical application obstacles of DBDs such as mass transfer of reactive species from gas phase to target pollutants, plasma source temperature elevation issue, and electrode corrosion (Jiang et al., 2014). Synthetic contaminated water (SCW) samples containing chemical contaminant (Sulfamethoxazole) and biological contaminant (*E. coli* K12) were prepared for plasma treatment. The plasma reactor is characterized and demonstrated for degrading various concentrations of SCW samples with chemical contaminant and biological contaminant. SMX degradation efficiency, degradation products, *E. coli* K12 inactivation efficiency, and corresponding energy yields were investigated using the plasma reactor.

2. Material and methods

2.1. Plasma reactor

The schematic of the plasma bubbling reactor is illustrated in Fig. 1a. As can be seen, the designed test reactor consists of a surface DBD plasma source and a hydrophobic polytetrafluoroethylene (PTFE) membrane (Sartorius Hydrophobic PTFE Membrane Filters, Type 11807, diameter 47 mm) with a 0.22 μm pore size to produce bubbles in the liquid when gas passes through. Bubbling is a simple and effective method to increase the interfacial area between gas phase and liquid phase by dispersing the DBD plasma activated gas into the liquid (Magureanu et al., 2008; Mok et al., 2008). Air is introduced from the bottom of the reactor and becomes activated when passing through the

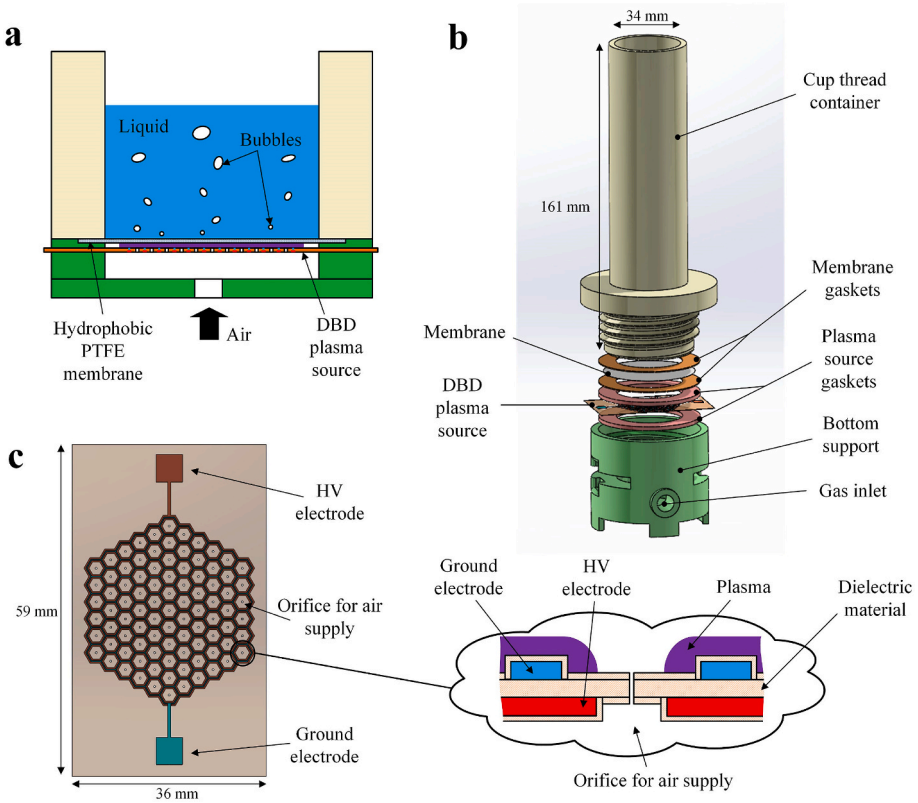

Fig. 1. DBD plasma reactor (a) Schematic of the plasma bubbling reactor. (b) Exploded view of the plasma reactor assembly. (c) DBD surface plasma source.

plasma region. The PTFE membrane is carefully placed so that it is close to plasma region.

The exploded view of the bubbling reactor assembly is shown in Fig. 1b. It consists of a cup thread container for liquid bubbling, a membrane, a surface DBD plasma source, gaskets, and a bottom support part with a compressed air gas inlet. The cup thread container has an inner diameter (ID) of 34 mm and an outer diameter (OD) of 40 mm, with a total height of 161 mm. The gaskets (OD 55 mm, ID 34 mm) are 0.5 mm thick for the membrane and 2 mm thick for the plasma source. Both the membrane and plasma source are sandwiched with gaskets and sealed with silicone glue to ensure air tightness when assembled. The membrane and plasma source sandwich structure can be conveniently replaced when needed during experiments. The bottom support part has a gas inlet hole for mounting a push-to-connect tube fitting. The assembled reactor has the dimensions around 200 mm × 70 mm × 70 mm (height × length × width), and the total mass of the reactor (including plasma source, membrane, gaskets, lead wires, and connectors) is around 220 g. Dry air is introduced through a mass flow controller (MC-series, Alicat Scientific) with flexible gas tube (RS FEP 140 tubing, OD 4 mm, ID 2.5 mm. Two side slots are also designed for electrode access and replacement of membrane module and plasma source module. The threads mount on the cup thread container and the bottom support part can provide sufficient compression force to ensure that there is no gas leakage during system operation. Both the cup thread container and the bottom support parts are 3D printed with clear resin using a Form 3+ printer (Formlabs).

The surface DBD plasma source consists of five layers: two electrode layers separated by a dielectric material base layer, and two cover layers on top of each electrode layer. As a plasma bubbling reactor requires injecting gas (air), a porous surface DBD plasma source has been developed with an orifice for air injection. As shown in Fig. 1c, a porous surface DBD plasma source consists of hexagonal electrode pattern with a total extension of 33 mm and a unit size of 2 mm for each individual hexagon. The hexagonal electrode pattern was chosen as it provides the largest area for uniform plasma generation at minimal electrode material (Jakob, 2022), see Supplementary Materials. The linewidth of the ground electrode is 0.2 mm and, therefore, smaller than the linewidth of the high voltage electrode with 0.8 mm to encourage plasma generation on the ground electrode side. Each centre of a hexagon has a 0.35 mm orifice to allow air injection. A schematic section view of one of the hexagonal elements is also presented in Fig. 1c. The dielectric polyimide substrate (75 μm thickness) has a 35 μm thick copper layer on each side, from which the electrode pattern will be etched. Both sides are covered with 25 μm polyimide cover lay (solder resist) as a protective layer between the highly energetic plasma region and the plasma source materials. Etching has the advantage of producing electrode patterns with high precision and providing pure metal (copper) as the electrode material.

2.2. Plasma characteristics

Fig. 2a shows the schematic diagram of the plasma source circuit. The circuit of the plasma source consists of a function generator, an audio amplifier, and a transformer. The function generator introduces the sinusoidal waveform within the audio frequency range at 1 V amplitude as the audio amplifier (Crown CDi DriveCore) input. With the help of the audio amplifier, the amplitude of the sinusoidal waveform is increased to 40–50 V. The AC signal output amplitude from the audio amplifier is then elevated by a step-up transformer (TRI-STAR 4967, turns ratio 1:360, Corona Magnetics, Inc.) to the kilovolt level, capable of driving the plasma source. The function generator used in the setup is the oscilloscope (Tektronix MDO34) integrated Arbitrary Function Generator. The electrical characteristics of the plasma are monitored through a high voltage probe (Tektronix P6015A), current probe (Pearson Model 6585), and a monitor capacitor (10 nF) to estimate the transferred charge.

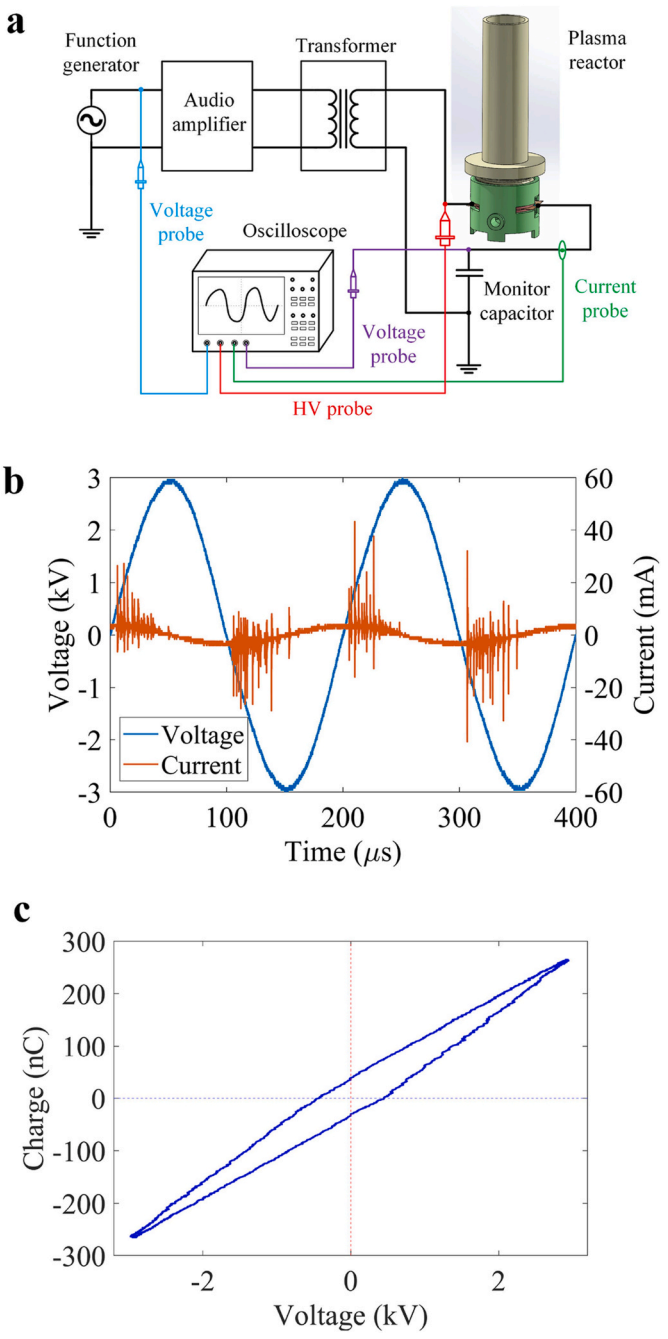

Fig. 2. Plasma source circuit characteristics (a) Diagram of the plasma source circuit and diagnostics. (b) Typical waveforms of current and voltage captured by oscilloscope. (c) Typical Lissajous figure for the DBD plasma source.

Fig. 2b presents the measured voltage and current of the plasma source during operation. The voltage follows the sinusoidal driving signal and has a peak-to-peak voltage of 6 kV at a fixed frequency of 5 kHz. On the current signal, the plasma discharge can clearly be identified through the superimposed high frequency and amplitude current peaks (micro discharges) in the negative and positive half period of the current measurement. Fig. 2c demonstrates the voltage-charge characteristics of the DBD plasma source, also known as the Lissajous figure which is used to obtain the discharge power based on the area within the curve. The monitor capacitor method is widely used for accurate estimation of the power consumptions of DBD plasma actuators in flow control applications (Ashpis et al., 2012). The obtained Lissajous graph has the shape of a parallelogram with blunt edges (almond shaped),

which is typical for surface DBD plasma sources compared to a sharp parallelogram-like curve, which is usually seen for volume DBD plasma sources. The electric energy consumed per voltage cycle can be estimated as the area within the Lissajous curve using the following equation:

$$E = \oint V(t)dQ \quad (1)$$

where $V(t)$ is the applied voltage of the surface DBD, Q is the transferred charge measured by the monitor capacitor. The discharge power can be derived using the following equation

$$P = fE = \frac{1}{T}E \quad (2)$$

in which f is the frequency of the AC signal, T is the period of the AC signal. The estimated energy per cycle is 0.2548 ± 0.0037 mJ, and the power of the plasma source operating at 5 kHz is 1.274 ± 0.018 W. In this study, the discharge energy per cycle and discharge power are estimated using the MATLAB codes.

The optical emission spectroscopy (OES) data and analysis of the DBD plasma source are demonstrated in Fig. 3; the experimental setup can be seen in Fig. S1 in the Supplementary Material. The second positive system (SPS) of N_2 is observed (Fig. 3a), which is common in air plasma discharges. The SPS of N_2 experimental spectra were compared to the modelled spectra from SpecAir (Burnette and Staack, 2020; Laux et al., 2003) shown in Fig. 3b. For the range of 350–360 nm spectrum, the modelled spectrum yields a rotational temperature of 380 K and a vibrational temperature of 1400 K. The difference between vibrational and rotational temperature indicates that the surface DBD is a highly non-equilibrium plasma.

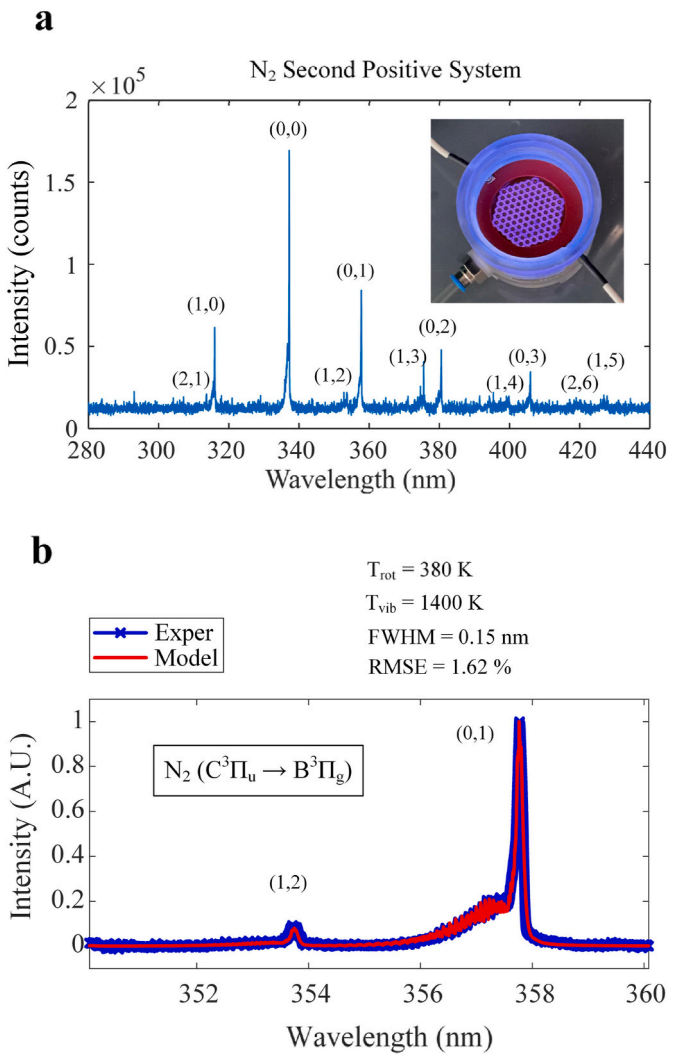

Fig. 3. Optical emission spectroscopy (OES) of the surface DBD plasma source and modelled spectra (a) Spectrum of the surface DBD from 280 nm to 440 nm. (b) Fitted spectrum from 350 to 360 nm.

2.3. Optimization of •OH radicals formation by gas flow rate

The indiscriminate hydroxyl (•OH) radicals with a higher oxidation potential are the vital oxidants in plasma water treatment, and the end products are less harmful or even harmless. The •OH radicals in plasma treated water solution mainly originate from two sources: dissolved from the gas phase, which is generated directly by air plasma (Kanazawa et al., 2011); and produced by the peroxone process (see reactions S1-S5 in the Supplementary Material) with plasma generated ozone and hydrogen peroxide (Rosenfeldt et al., 2006; Staehelin and Holgné, 1982). Some of the directly generated •OH radicals near gas/liquid interface diffuse into water within a short diffusion length and will be converted into hydrogen peroxide which is one of the long-lived species. This is also the major pathway to hydrogen peroxide formation (Mededovic and Locke, 2007).

N,N-Dimethyl-4-Nitrosoaniline ($C_8H_{10}N_2O$, Sigma-Aldrich, USA) has been used as a probe compound for detection of hydroxyl radicals (•OH-R) and shows little reaction with singlet oxygen ($^1O_2$), superoxide anions (O_2^-), and peroxyl compounds (R−O−O−R) (Lee et al., 2018). The •OH radicals were indirectly quantified based on the assumption that the hydroxyl radicals production by non-thermal plasma is very selective to N,N-Dimethyl-4-Nitrosoaniline, therefore, able to oxidize it in aqueous solution (Li et al., 2009). It is an indirect indicator of •OH radical formation, presenting peak absorption wavelength of 440 nm. The absorption wavelength measurement was performed on the plasma treated solution using a UV–Vis spectrophotometer (Cary 60, Agilent Technology, USA). Absorbance was then measured and converted to the concentration value of the probe detection of •OH radical using a calibration curve. The plasma discharge applied voltage was set at 6 kV based on MB degradation experiments to ensure competitive reactor performance shown in Figure S2 and Figure S3, fully ignition of surface DBD, and the plasma source lifetime. Dry air, mainly composed by Oxygen (21%) and Nitrogen (78%), was used to feed the DBD reactor and reactive species generated from the DBD reactor were transferred to the aqueous solution (working volume of 100 mL) through the membrane gas diffuser. The initial concentration of N,N-Dimethyl-4-Nitrosoaniline was 10 mg/L. Air flowrate experiments were performed by adjusting it (0.5, 1.0, 1.5, 2.0 and 4.0 L/min) over a run of 1 h (each condition). Samples were taken for analysis at 1, 3, 5, 7, 10, 15, 20, 30, 45, and 60 min.

2.4. Chemical and biological contaminants

Two sets of SCW were prepared: a chemical-contaminated set and a bio-contaminated set. The chemical-contaminated SCW was prepared using dechlorinated tap water to which a mixture of known concentration of SMX was added (SCW sample concentrations: 0.5, 5.0 and 50 mg/L). SMX standard (purity ≥99.0%) was purchased from Sigma-Aldrich, UK. HPLC grade acetonitrile and methanol were obtained from Fisher Scientific, UK. Stock solution standard was prepared in methanol at 1 mg/mL. A working solution was prepared by diluting the stock solutions in ultrapure water to 1 mg/L. The stock solution was stored at −20 °C and working solutions were preserved at 4 °C.

The second set of SCW with bio-contaminant was prepared using dechlorinated tap water and *Escherichia coli* (*E. coli* K12 ATCC 11775 from Fisher Scientific Ltd) at concentrations of 10^2, 10^4 and 10^8 Colony Forming Units (CFU) per mL. The dechlorination process was performed by allowing the water to stand for 24 h to dechlorinate naturally. It is

important to mention that plasma discharge, air flow rate and sample volume were kept the same as in Section 2.3. The airflow rate applied was 2.0 standard litre per minute (SLPM), which represented the best condition observed in the optimization of •OH radical formation test.

2.5. Liquid chromatography with tandem mass spectrometry (LC-MS/MS)

Sulfamethoxazole belongs to the sulphonamide group and was selected as a target antibiotic based on three main criteria.

1) Presence in final treated drinking water (Boleda et al., 2014);
2) Occurrence in tap water at concentrations up to 21.2 ng/L (Leung et al., 2013);
3) Availability of a reliable analysis method (Xu et al., 2020, 2021).

LC-MS/MS analyses were carried out to determine the extent of antibiotic degradation. The LC-MS/MS system and protocol used in this study are described in Supplementary Material.

2.6. Quantification of E. coli K12

Detection of coliforms is used as an indicator of sanitary quality of water. Hence, *E. coli* strain designation K12 was selected as a target microorganism based on two main criteria.

1) *E. coli* is widely reported as an indicator of faecal contamination (Baird et al., 2017);
2) It represents the genetically best understood living organism (Kuhnert et al., 1995).

Coliform agar (Chromocult ®–Merk) was prepared according to manufacturer's instructions. Samples were prepared, homogenized, and decimally diluted. One hundred μL aliquots of each dilution were transferred to Petri dishes. Plates were inverted (24, 48 and 72 h) and incubated at 35 °C. Plates were then examined under a magnifying lens and with illumination; purple-red colonies that are 0.5 mm or larger in diameter were counted. The cut-off number was between 25 and 250 colonies. The number of CFU on the countable plate is multiplied by the final dilution factor and divided by the volume of culture plated in mL to obtain the number of CFU per mL of the original sample.

3. Results and discussion

3.1. Effects of air flow rate for the plasma reactor

Fig. 4a presents the target substance degradation at different air flow rates after DBD plasma treatment (V_{pp} = 6.0 kV, 5 kHz). The concentration of N,N-Dimethyl-4-Nitrosoaniline decayed exponentially and followed first-order reaction kinetics. The overall trend of the observed rate constant, k_{obs}, increased with rising air flow rate and it approached to a threshold after reaching a specific flow rate. The highest rate constant observed was 0.0062 s^{-1} for both 2.0 SLPM and 4.0 SLPM within the first 7 min treatment (representing more than 80% conversion in concentration), as shown in the first-order plots of N,N-Dimethyl-4-Nitrosoaniline degradation in Fig. 4b. The highest observed rate constant, k_{obs} is better than the highest reported value (k_{obs} = 0.104 min^{-1} = 0.00173 s^{-1}) using a non-thermal plasma device to treat a 9 mg/L N,N-Dimethyl-4-Nitrosoaniline solution at a 7 L/min air flow rate (Lee et al., 2018). Since air flow rate of 4.0 SLPM leads to splashing of solution droplets to the container inner wall and overflow due to strong bubbling effects, the suggested better air flow rate is 2.0 SLPM. This also demonstrated that the air flow rate cannot be augmented infinitely, as the residence time of the radicals contained in the bubble would be shortened with a higher bubbling rate (Tang et al., 2018). Fig. S4 provides reference bubble size measurements for the reactor operating at different air flow rates with 100 mL of deionized water. The median of the equivalent radius of the bubbles grows with increasing air flow rate. The choice of air flow rate would be constrained by the reactor scale and its ventilation capacity.

3.2. Decontamination of chemical contaminant

The samples have been analyzed using a LC-MS/MS instrument programmed to acquire MS data in data dependent mode. The sample was injected on the reversed-phase LC column, where degradation products and SMX were chromatographically separated and the effluent from the LC column was continuously introduced into a HESI source of Q Exactive mass spectrometer. Data dependent mode allowed acquisition of a full mass spectrum, followed by selection of the 8 most intense singly charged ions from the MS full scan for MS/MS fragmentation. This allowed characterization of degradation products of SMX based on their accurate mass measurements and MS/MS mass spectra. Fig. 5 shows the total ion current (TIC) chromatograms for different plasma treatment times (T0 = 0 min, T3 = 5 min, T5 = 10 min, T6 = 15 min, T7 = 20 min, T8 = 30 min, T9 = 45 min, T10 = 60 min), which demonstrate the progress of degradation of SMX. SMX eluted from the C18 column at the retention time 4.27 min. The information of LC-MS/MS method validation and the ESI mass spectrum of SMX is shown in Supplementary Materials, Fig. S5. As can be seen from Fig. 5, there was significant decrease in the SMX chromatographic peak around 4.28 min and the generation of several degradation products upon treatment of SMX for 60 min.

As demonstrated in Fig. 6a, SMX in the SCW is below the limit of detection (LOD) after 7 min and 30 min for initial concentrations of 0.5 mg/L and 5 mg/L respectively. The total amount of the antibiotic

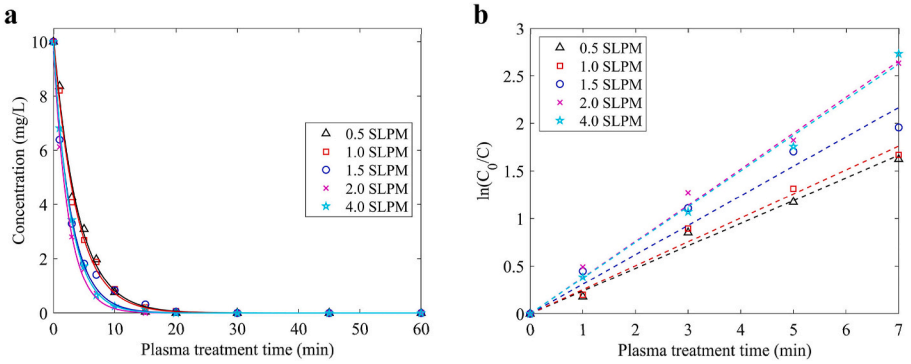

Fig. 4. N,N-Dimethyl-4-Nitrosoaniline degradation (a) Degradation over plasma treatment time at different flow rates with plasma applied voltage V_{pp} = 6.0 kV, frequency f = 5 kHz. (b) First-order plots of N,N-Dimethyl-4-Nitrosoaniline degradation as a function of plasma treatment time, dashed lines are least-squares regression lines.

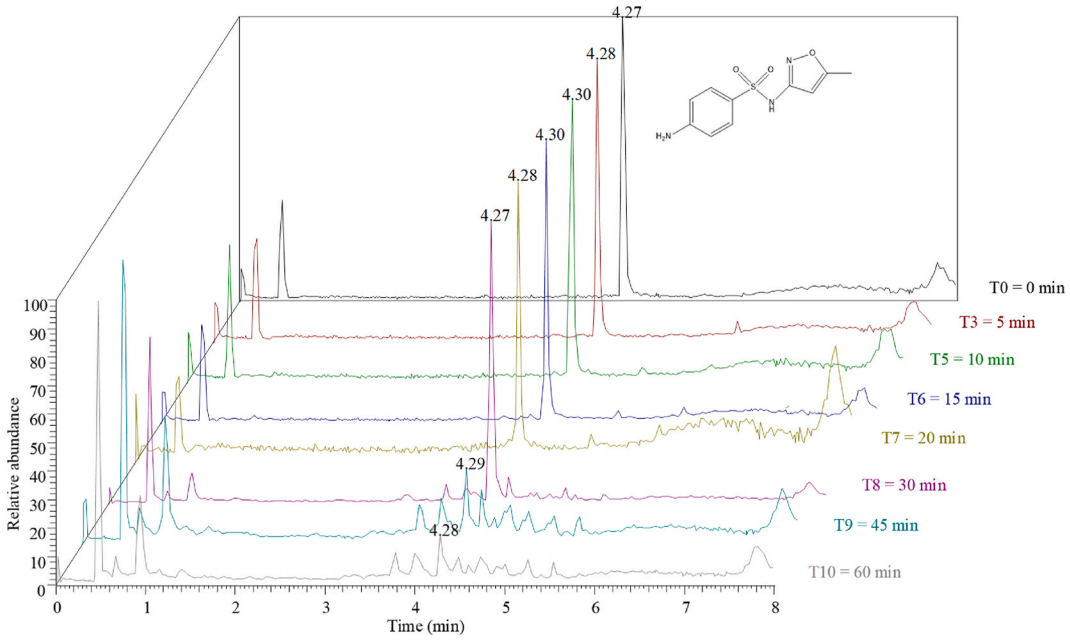

Fig. 5. Base peak chromatograms for various plasma treatment times of SMX: T0 at 0 min (black line), T3 at 5 min (brown line), T5 at 10 min (green line), T6 at 15 min (blue line), T7 at 20 min (light green line), T8 at 30 min (dark purple line), T9 at 45 min (light green line), T10 at 60 min (light grey line). Initial SMX solution concentration = 50 mg/L; initial pH = 7; air flowrate = 2.0 SLP M; applied voltage V_{pp} = 6.0 kV; sample volume = 100 mL.

removed by plasma is significantly larger for higher initial concentration. With the plasma source power at 1.274 W, the energy yields for the removal of SMX are 0.34 g/kWh, 0.78 g/kWh, and 3.92 g/kWh, respectively.

The first-order plots of SMX degradation as a function of treatment time are illustrated in Fig. 6b. The experimental data are non-linear, and the rate constant (the slope in Fig. 6b) of SMX decontamination depends on the initial concentration of the antibiotic in SCW: the removal is slower with increasing initial concentration. One possible explanation is that the concentrations of reactive species generated during plasma-liquid interaction are unable to ensure a pure first-order kinetic since the active species are involved in both the oxidation of the initial parent compound and its reaction products (Magureanu et al., 2010).

The antibiotic degradation dependence on initial concentration have been reported in different publications (Guo et al., 2019; He et al., 2014; Kim et al., 2013; Rong and Sun, 2014; Rong et al., 2014; Wang et al., 2018). The general trend, main degradation paths, and energy yield at various removal percentages (mainly 90% removal) were concisely summarized in a critical review on non-thermal plasma treatment of water contaminated with antibiotics (Magureanu et al., 2021). Since the figure-of-merit $Y_{50\%}$ depends on chemical species in solution, initial concentration, feeding gas, gas flow rate, and the reactor design, it is challenging to compare reactor designs in different dimensions. The $Y_{50\%}$ of SMX degradation using an argon plasma jet in nanopure water (1 mg/L) was around 6.4×10^{-4} g/kWh (Rodriguez et al., 2022). In another DBD plasma reactor for SMX (initial concentration 5 mg/L) degradation, the $Y_{50\%}$ was calculated to be 2.30 g/kWh with an air flow rate of 2.0 L/min, and 3.09 g/kWh with an air flow rate of 0.5 L/min (Kim et al., 2013). Later, the $Y_{50\%}$ of the reactor was improved to around 49.3 g/kWh by bubbling into the antibiotic solution via three ceramic gas diffusers (Kim et al., 2015) at air flow rate 0.5 L/min. The $Y_{50\%}$ increased by almost 15 times with bubbling enhancement (the number of ceramic gas diffusers increased from 1 to 3) combined with discharge power adjustment in air (2.82 W, 60 Hz). While the specifics regarding ceramic gas diffusers and the resulting bubble sizes were not elaborated upon, this enhancement in reactor performance highlights the benefits of bubbling and warrants further investigation.

To quantify the efficiencies of different plasma reactors, the energy yield at 50% conversion of the pollutant ($Y_{50\%}$) was proposed (Malik, 2010) in the plasma treatment community as a figure-of-merit. The energy yield needed to remove 50% of SMX with an initial concentration of 0.5 mg/L after 3 min of plasma treatment resulted in $Y_{50\%}$ = 0.39 g/kWh. For an initial concentration of 5.0 mg/L SMX sample, the 50% removal is fulfilled after 10 min of plasma treatment, achieving $Y_{50\%}$ = 1.16 g/kWh. With interpolation of the treatment time dependent concentration of the 50 mg/L SMX sample, the $Y_{50\%}$ is estimated to be 8.12 g/kWh. These results demonstrate that the $Y_{50\%}$ grows with the increasing initial concentration of SMX in the SCW. Enhanced efficiency of plasma treatment is expected for concentrated effluents, proving that contaminated water should be treated at the source of pollution (Magureanu et al., 2021).

Another noteworthy figure-of-merit termed as electrical energy per order (EE/O, electrical energy required to bring about the degradation of a contaminant concentration by one order of magnitude in 1 m^3 of contaminated water or air) is recommended for direct comparison of various plasma reactor efficiencies, since it is used in the conventional advanced oxidation water treatment community for low initial concentrations (i.e. cases that are overall first-order reactions) (Bolton et al., 1996). The estimated EE/O for 0.5 mg/L, 5.0 mg/L, and 50 mg/L SMX samples are 1.519, 3.881, and 6.272 kWh/m^3 per order respectively. Compared to 3.22×10^5–1.89×10^6 kWh/m^3 per order in another SMX plasma degradation in synthetic urine (Rodriguez et al., 2022) with 1 mg/L concentration, this reactor performance is distinctive. Among total of 48 plasma reactors and other different advanced oxidation processes (such as electrochemical and photo-Fenton) in the critical review for water treatment (Miklos et al., 2018), the EE/O values of this plasma reactor are below their average value, with 0.5 mg/L case outperforming 95% of the listed plasma reactors as shown in Fig. S6.

Key degradation products of SMX using plasma treatment method have been previously reported in detail (Bilea et al., 2024; Kim et al., 2015; Magureanu et al., 2021). The degradation products identified in our data are summarized in Supplementary Material Table S1. These products will be referred to by the similar notation applied in the study by Bilea et al., which is comprised of: S-sulfamethoxazole; a number representing the nominal mass of the compound; a,b,c – for position isomers of the respective structures (Bilea et al., 2024).

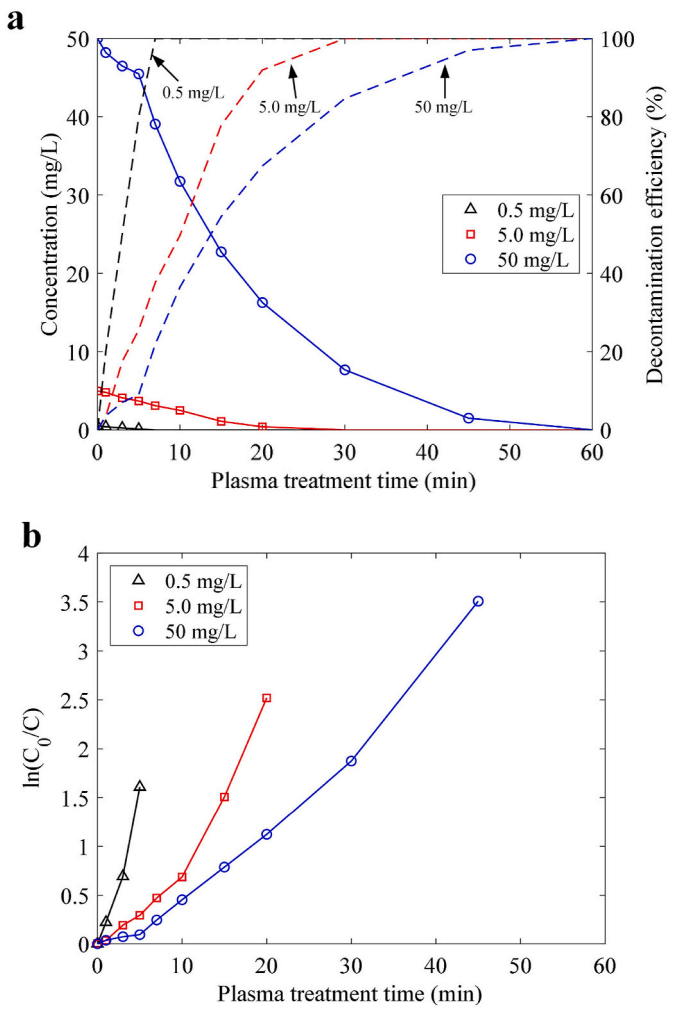

Fig. 6. Degradation of chemical contaminants (a) Decontamination of SMX concentration (solid line with markers) and efficiency (dashed line) at initial concentrations of 0.5 mg/L, 5 mg/L, and 50 mg/L over plasma treatment time. (b) First-order plots of SMX degradation as a function of treatment time for initial concentrations of 0.5 mg/L, 5 mg/L, and 50 mg/L.

The identification of SMX degradation products was based on their accurate mass measurements and MS/MS mass spectra. The reconstructed ion chromatograms (RICs) for those key degradation products are shown in Fig. S7. The proposed degradation paths of SMX are illustrated in Fig. 7. Path 1 starts with the attack of •OH on the C6 atom of the isoxazole ring, generating S269a in two steps: the cleavage of the double bond leaving C2 atom with an unpaired electron; and reformation of the double bond due to the •OH driven hydrogen abstraction from C6. Subsequently, the reaction of O_2 with the C2 carbon-centred radical induces the formation of di-hydroxylated S287. Alternatively, direct cleavage of the S8-N7 bond of S269a can produce S173 and S114. Additionally, the reaction of O_2 with the C2 carbon-centred radical can generate S132. While the direct cleavage of the S-N bond of S287 has been reported (Bilea et al., 2024), the simultaneous presence of S173 (5–30 min) and S132 (45–60 min) was not observed in our case. Path 2 commences with the direct cleavage of the S8-N7 bond of SMX, resulting in the formation of S173 and S98. Similar to Path 1, •OH attack on the C6 atom converts the isoxazole ring of S98 to S114. Further on, di-hydroxylated S132 is generated through the reaction of O_2 with S114. Path 3 commences with the hydroxylation of the benzene ring triggered by •OH attack, thereby generating the S269bc isomers. Through the hydroxylation mechanism, di-hydroxylated S285 is produced via sequential •OH attacks on the benzene ring. The ozone's attack on the amine group of S269bc leads to the formation of S283a. Further oxidation of this compound can result in the elimination of the nitrogen-containing group and the formation of S270 diol. Path 4 involves the cleavage of the C11-S8 bond, possibly due to •OH attacking the sulfur atom, leading to the formation of S178 sulfamic acid and an aniline radical. S178 may originate from any intermediate degradation products from Path 3. Further oxidation of all resulted intermediate products leads to the formation of short chain carboxylic acids (formic acid, acetic acid, oxalic acid), nitrate, ammonium, sulphate (Kim et al., 2015; Li et al., 2020; Magureanu et al., 2021; Rong and Sun, 2014). In addition, temporal variations of pH affecting potability of the treated water (Allabakshi et al., 2023; Li et al., 2022), electrical conductivity, UV absorption pattern and total organic carbon need to be monitored during the future experiments.

3.3. Decontamination of biological contaminant

As summarized in the plasma medicine review (Weltmann and Von Woedtke, 2017), ROS (Joshi et al., 2011; Pavlovich et al., 2013) and RNS (Oehmigen et al., 2011) generated in or transferred into the liquid phase play a dominating role in damaging bacterial cell components such as proteins, lipids, and DNA, leading to cell inactivation. The formation of secondary reactive species such as peroxynitrite ($ONOO^-$), can further contribute to bacterial inactivation (Lukes et al., 2014; Van Gils et al., 2013). The electric fields generated by the plasma can induce electroporation (Bermúdez-Aguirre et al., 2013) in the cell membrane, disrupt cell membrane integrity and cause structural damage to the cell wall, leading to cell death. Fig. 8a shows that *E. coli* K12 was completely inactivated after 10 min and 45 min for initial *E. coli* concentrations of 10^2 CFU/mL and 10^4 CFU/mL, respectively. *E. coli* concentration of 10^8 CFU/mL achieved a 5-log reduction after 60 min of treatment. This indicates that the plasma system was effective in inactivating *E. coli* K12.

A comparison of this plasma reactor performance on *E. coli* inactivation with experiments in other research investigations (Dors et al., 2008; Estifaee et al., 2019; Joshi et al., 2011; Nguyen et al., 2019; Oehmigen et al., 2011; Patinglag et al., 2021; Pavlovich et al., 2013; Ziuzina et al., 2013) is summarized in the Supplementary Material Table S2. The energy efficiency of this plasma reactor is 117.2 CFU/J (10^2 CFU/mL), 2689.1 (10^4 CFU/mL), and 8394370 CFU/J (10^8 CFU/mL), demonstrating outstanding performance for *E. coli* inactivation at different concentrations. The first-order plots of *E. coli* K12 are also non-linear as shown in Fig. 8b. Unlike the degradation of SMX where the initial rate constant is smaller with increasing initial concentration, the rate constant within the first 10 min treatment time of the 10^8 CFU/mL case is higher compared to cases with initial concentration 10^2 CFU/mL and 10^4 CFU/mL, owing to the complexity of bacteria plasma treatment (Estifaee et al., 2019). As the bacteria used in this project belong to category 1 (i.e. non-pathogenic), future research needs to test the proposed system against pathogenic and antibiotic resistant bacteria such as methicillin-resistant *Staphylococcus aureus* (MRSA).

4. Conclusion

A plasma bubbling batch reactor with a surface DBD plasma source was designed and manufactured for water treatment. The SMX degradation results indicated that the degradation process does not follow the first-order kinetic model, and the reaction rate dwindled with increasing initial concentration. The figure-of-merit $Y_{50\%}$ for the SMX test was also initial concentration dependent, the plasma reactor performed better with a higher concentration contaminant level among the tested concentrations, achieving the highest value of 8.12 g/kWh for 50 mg/L. Identification of key degradation products through LC-MS/MS analysis revealed insights into the degradation pathway of SMX, underscoring the pivotal role of •OH radicals in driving the SMX degradation process. The inactivation of the biological contaminant *E. coli* K12 did not follow the first-order kinetic model; a 5-log reduction is achieved with an initial

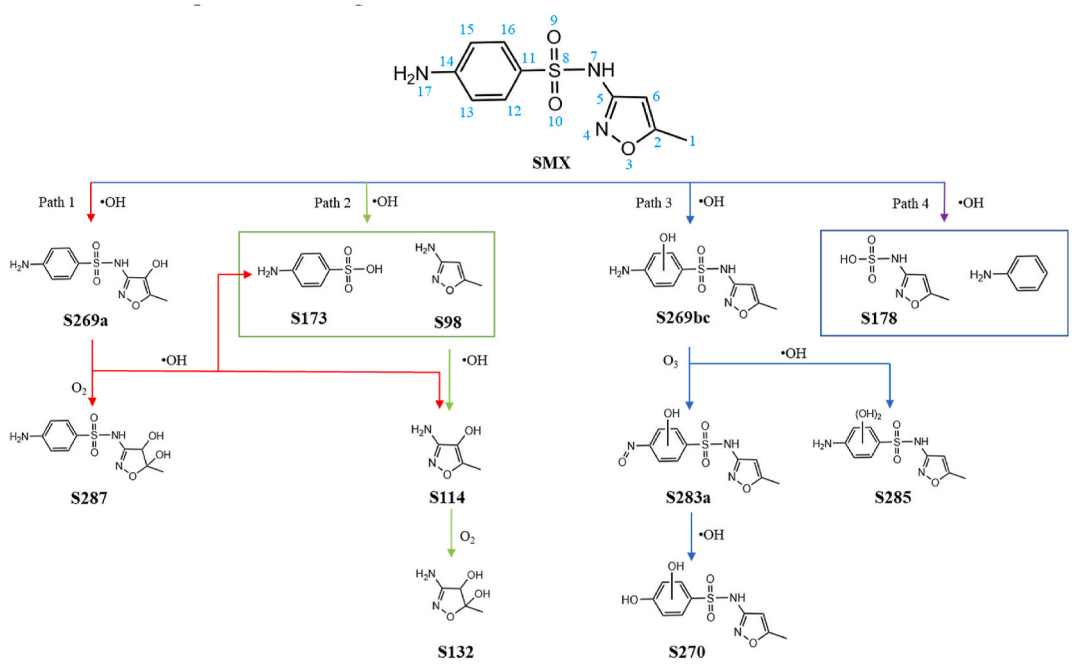

Fig. 7. Proposed degradation paths of SMX.

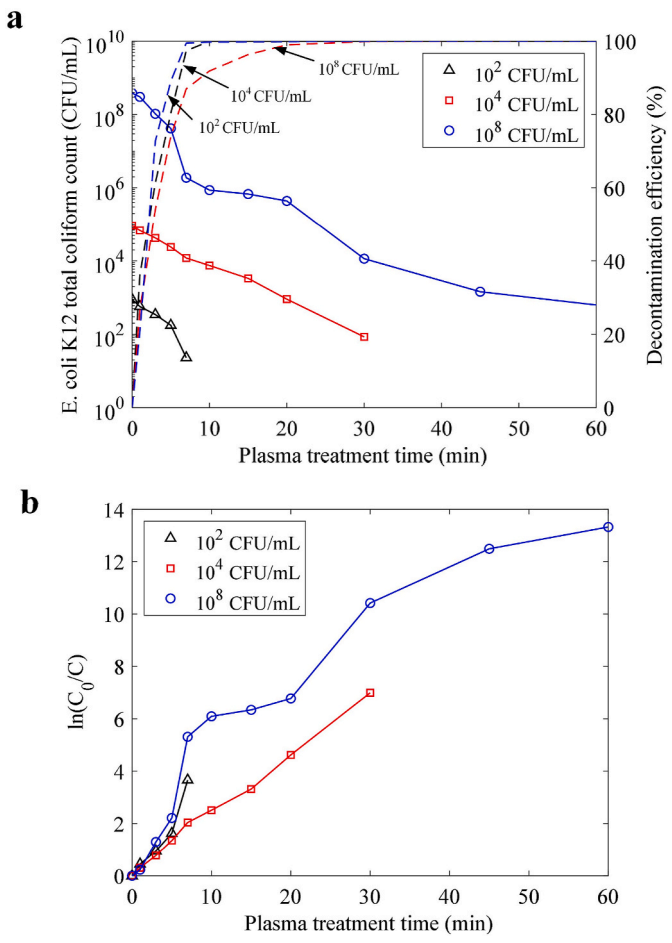

Fig. 8. Degradation of biological contaminants *E. coli* K12 (a) Decontamination of *E. coli* K12 at initial concentrations of 10^2 CFU/mL, 10^4 CFU/mL, and 10^8 CFU/mL. (b) First-order plots of *E. coli* K12 total coliform count over plasma treatment time at initial concentrations of 10^2 CFU/mL, 10^4 CFU/mL, and 10^8 CFU/mL.

concentration of *E. coli* K12 at 10^8 CFU/mL after 60 minutes of treatment, and the rate constant during the first 10 min is higher compared to cases with 10^2 CFU/mL and 10^4 CFU/mL.

The design of this batch reactor with plasma bubbling is promising for decontaminating both chemical and biological contaminants with a relatively low applied voltage. The tested results using SCW samples make it encouraging not only for in-situ water treatment in aerospace applications, but also for solving water pollution issues on earth. The scaled-up version of this type of reactor will be developed in the future with a closed-loop configuration to enhance the reactor efficiency by making most use of the long-lived species generated in the plasma. Future research should focus on quantifying the contribution of individual reactive species for chemical contaminant degradation and biological contaminant inactivation, the potability of the treated water, and reactor optimizations.

Funding

This work was supported by the UK Space Agency (UKSAG22_0006).

CRediT authorship contribution statement

Xin Tang: Writing – review & editing, Writing – original draft, Visualization, Resources, Project administration, Methodology, Investigation, Formal analysis. **Antônio D.N. Ferraz Júnior:** Writing – review & editing, Visualization, Validation, Resources, Project administration, Methodology, Investigation, Formal analysis, Data curation. **Kersti Karu:** Writing – review & editing, Validation, Software, Resources, Methodology, Investigation, Formal analysis, Data curation. **Luiza C. Campos:** Writing – review & editing, Validation, Supervision, Resources, Project administration, Methodology, Investigation, Funding acquisition, Conceptualization. **Minkwan Kim:** Writing – review & editing, Visualization, Validation, Supervision, Resources, Project administration, Methodology, Funding acquisition, Conceptualization.

Declaration of competing interest

The authors declare that they have no known competing financial interests or personal relationships that could have appeared to influence

the work reported in this paper.

Data availability

Data will be made available on request.

Acknowledgements

The authors express their gratitude for the invaluable support provided by Dr Melisa Canales (University College London) throughout the microbial analysis and Dr Naigui Shang (University of Southampton) for the reactor solution temperature measurement.

Appendix A. Supplementary data

Supplementary data to this article can be found online at https://doi.org/10.1016/j.jenvman.2024.122574.

References

Al Aukidy, M., Verlicchi, P., Jelic, A., Petrovic, M., Barcelò, D., 2012. Monitoring release of pharmaceutical compounds: occurrence and environmental risk assessment of two WWTP effluents and their receiving bodies in the Po Valley. Italy. Sci. Total Environ. 438, 15–25. https://doi.org/10.1016/j.scitotenv.2012.08.061.

Allabakshi, S.M., Srikar, P.S.N.S.R., Gangwar, R.K., Maliyekkal, S.M., 2023. Treatment of azo, direct, and reactive dyes in surface dielectric barrier discharge: valorization of effluent, the influence of wastewater characteristics, and plasma modeling by Stark broadening technique. J. Water Process Eng. 56, 104503. https://doi.org/10.1016/j.jwpe.2023.104503.

Allabakshi, S.M., Srikar, P.S.N.S.R., Gangwar, R.K., Maliyekkal, S.M., 2022. Feasibility of surface dielectric barrier discharge in wastewater treatment: spectroscopic modeling, diagnostic, and dye mineralization. Sep. Purif. Technol. 296, 121344. https://doi.org/10.1016/j.seppur.2022.121344.

Ashpis, D.E., Laun, M.C., Griebeler, E.L., 2012. Progress toward accurate measurements of power consumptions of DBD plasma actuators. In: 50th AIAA Aerospace Sciences Meeting Including the New Horizons Forum and Aerospace Exposition. https://doi.org/10.2514/6.2012-823.

Baird, R.B., Eaton, A.D., Rice, E.W., Bridgewater, L.L., 2017. Standard Methods for the Examination of Water and Wastewater, 23rd ed. American Public Health Association, American Water Works Association, Water Environment Federation, Washington, DC.

Benotti, M.J., Trenholm, R.A., Vanderford, B.J., Holady, J.C., Stanford, B.D., Snyder, S. A., 2009. Pharmaceuticals and endocrine disrupting compounds in U.S. drinking water. Environ. Sci. Technol. 43, 597–603. https://doi.org/10.1021/es801845a.

Bermúdez-Aguirre, D., Wemlinger, E., Pedrow, P., Barbosa-Cánovas, G., Garcia-Perez, M., 2013. Effect of atmospheric pressure cold plasma (APCP) on the inactivation of *Escherichia coli* in fresh produce. Food Control 34, 149–157. https://doi.org/10.1016/j.foodcont.2013.04.022.

Bilea, F., Bradu, C., Cicirma, M., Medvedovici, A.V., Magureanu, M., 2024. Plasma treatment of sulfamethoxazole contaminated water: intermediate products, toxicity assessment and potential agricultural reuse. Sci. Total Environ. 909, 168524. https://doi.org/10.1016/j.scitotenv.2023.168524.

Boleda, M.R., Alechaga, É., Moyano, E., Galceran, M.T., Ventura, F., 2014. Survey of the occurrence of pharmaceuticals in Spanish finished drinking waters. Environ. Sci. Pollut. Res. 2118 21, 10917–10939. https://doi.org/10.1007/S11356-014-2885-9, 2014.

Bolton, J.R., Bircher, K.G., Tumas, W., Tolman, C.A., 1996. Figures-of-Merit for the technical development and application of advanced oxidation processes. J. Adv. Oxid. Technol. 1, 13–17. https://doi.org/10.1515/jaots-1996-0104.

Bradu, C., Kutasi, K., Magureanu, M., Puač, N., Živković, S., 2020. Reactive nitrogen species in plasma-activated water: generation, chemistry and application in agriculture. J. Phys. D Appl. Phys. 53, 223001. https://doi.org/10.1088/1361-6463/ab795a.

Brain, R.A., Ramirez, A.J., Fulton, B.A., Chambliss, C.K., Brooks, B.W., 2008. Herbicidal effects of sulfamethoxazole in Lemna gibba: using p-aminobenzoic acid as a biomarker of effect. Environ. Sci. Technol. 42, 8965–8970. https://doi.org/10.1021/es801611a.

Brisset, J.L., Pawlat, J., 2016. Chemical effects of air plasma species on aqueous solutes in direct and delayed exposure modes: discharge, post-discharge and plasma activated water. Plasma Chem. Plasma Process. 36, 355–381. https://doi.org/10.1007/s11090-015-9653-6.

Burnette, M., Staack, D., 2020. Development of a substrate-invariant 2-D array of nanosecond-pulsed streamer discharges. Plasma Res. Express 2, 015001. https://doi.org/10.1088/2516-1067/ab640f.

Diaz, A.M., Li, W., Irwin, T.D., Calle, L.M., Callahan, M.R., 2019. Investigation of biofilm formation and control for spacecraft-an early literature review. In: 49th International Conference on Environmental Systems. Boston, Massachusetts.

Dors, M., Metel, E., Mizeraczyk, J., Marotta, E., 2008. Pulsed corona discharge in water for coli bacteria inactivation. In: 2008 IEEE International Conference on Dielectric Liquids, ICDL 2008. https://doi.org/10.1109/ICDL.2008.4622538.

Estifaee, P., Su, X., Yannam, S.K., Rogers, S., Thagard, S.M., 2019. Mechanism of E. coli inactivation by direct-in-liquid electrical discharge plasma in low conductivity solutions. Sci. Rep. 91 (9), 1–12. https://doi.org/10.1038/s41598-019-38838-7, 2019.

Foster, J.E., 2017. Plasma-based water purification: challenges and prospects for the future. Phys. Plasmas 24, 055501. https://doi.org/10.1063/1.4977921.

Gorelova, V., Ambach, L., Rébeillé, F., Stove, C., Van Der Straeten, D., 2017. Folates in plants: research advances and progress in crop biofortification. Front. Chem. https://doi.org/10.3389/fchem.2017.00021.

Guo, H., Jiang, N., Wang, H., Lu, N., Shang, K., Li, J., Wu, Y., 2019. Pulsed discharge plasma assisted with graphene-WO_3 nanocomposites for synergistic degradation of antibiotic enrofloxacin in water. Chem. Eng. J. 372, 226–240. https://doi.org/10.1016/j.cej.2019.04.119.

He, D., Sun, Y., Xin, L., Feng, J., 2014. Aqueous tetracycline degradation by non-thermal plasma combined with nano-TiO_2. Chem. Eng. J. 258, 18–25. https://doi.org/10.1016/j.cej.2014.07.089.

Jakob, H., 2022. Development of Scalable and Exible Non-thermal Dielectric Barrier Discharge Systems for Novel Low-Temperature Plasma Applications. University of Southampton.

Jiang, B., Zheng, J., Qiu, S., Wu, M., Zhang, Q., Yan, Z., Xue, Q., 2014. Review on electrical discharge plasma technology for wastewater remediation. Chem. Eng. J. 236, 348–368. https://doi.org/10.1016/j.cej.2013.09.090.

Joshi, S.G., Cooper, M., Yost, A., Paff, M., Ercan, U.K., Fridman, G., Friedman, G., Fridman, A., Brooks, A.D., 2011. Nonthermal dielectric-barrier discharge plasma-induced inactivation involves oxidative DNA damage and membrane lipid peroxidation in *Escherichia coli*. Antimicrob. Agents Chemother. 55, 1053–1062. https://doi.org/10.1128/aac.01002-10.

Kanazawa, S., Kawano, H., Watanabe, S., Furuki, T., Akamine, S., Ichiki, R., Ohkubo, T., Kocik, M., Mizeraczyk, J., 2011. Observation of OH radicals produced by pulsed discharges on the surface of a liquid. Plasma Sources Sci. Technol. 20, 034010. https://doi.org/10.1088/0963-0252/20/3/034010.

Kim, K.S., Kam, S.K., Mok, Y.S., 2015. Elucidation of the degradation pathways of sulfonamide antibiotics in a dielectric barrier discharge plasma system. Chem. Eng. J. 271, 31–42. https://doi.org/10.1016/J.CEJ.2015.02.073.

Kim, K.S., Yang, C.S., Mok, Y.S., 2013. Degradation of veterinary antibiotics by dielectric barrier discharge plasma. Chem. Eng. J. 219, 19–27. https://doi.org/10.1016/J.CEJ.2012.12.079.

Kuhnert, P., Nicolet, J., Frey, J., 1995. Rapid and accurate identification of *Escherichia coli* K-12 strains. Appl. Environ. Microbiol. 61, 4135–4139. https://doi.org/10.1128/AEM.61.11.4135-4139.1995.

Laux, C.O., Spence, T.G., Kruger, C.H., Zare, R.N., 2003. Optical diagnostics of atmospheric pressure air plasmas. Plasma Sources Sci. Technol. 12, 125–138. https://doi.org/10.1088/0963-0252/12/2/301.

Lee, D., Lee, J.C., Nam, J.Y., Kim, H.W., 2018. Degradation of sulfonamide antibiotics and their intermediates toxicity in an aeration-assisted non-thermal plasma while treating strong wastewater. Chemosphere 209, 901–907. https://doi.org/10.1016/J.CHEMOSPHERE.2018.06.125.

Leung, H.W., Jin, L., Wei, S., Tsui, M.M.P., Zhou, B., Jiao, L., Cheung, P.C., Chun, Y.K., Murphy, M.B., Lam, P.K.S., 2013. Pharmaceuticals in tap water: human health risk assessment and proposed monitoring framework in China. Environ. Health Perspect. 121, 839–846. https://doi.org/10.1289/EHP.1206244.

Li, H., Li, T., He, S., Zhou, J., Wang, T., Zhu, L., 2020. Efficient degradation of antibiotics by non-thermal discharge plasma: highlight the impacts of molecular structures and degradation pathways. Chem. Eng. J. 395, 125091. https://doi.org/10.1016/J.CEJ.2020.125091.

Li, M., Feng, C., Hu, W., Zhang, Z., Sugiura, N., 2009. Electrochemical degradation of phenol using electrodes of Ti/RuO_2–Pt and Ti/IrO_2–Pt. J. Hazard Mater. 162, 455–462. https://doi.org/10.1016/J.JHAZMAT.2008.05.063.

Li, W., Zhou, Renwu, Zhou, Rusen, Weerasinghe, J., Zhang, T., Gissibl, A., Cullen, P.J., Speight, R., Ostrikov, K., 2022. Insights into amoxicillin degradation in water by non-thermal plasmas. Chemosphere 291 (Ken), 132757. https://doi.org/10.1016/J.CHEMOSPHERE.2021.132757.

Lucas, D., Badia-Fabregat, M., Vicent, T., Caminal, G., Rodríguez-Mozaz, S., Balcázar, J. L., Barceló, D., 2016. Fungal treatment for the removal of antibiotics and antibiotic resistance genes in veterinary hospital wastewater. Chemosphere 152, 301–308. https://doi.org/10.1016/j.chemosphere.2016.02.113.

Lukes, P., Dolezalova, E., Sisrova, I., Clupek, M., 2014. Aqueous-phase chemistry and bactericidal effects from an air discharge plasma in contact with water: evidence for the formation of peroxynitrite through a pseudo-second-order post-discharge reaction of H_2O_2 and HNO_2. Plasma Sources Sci. Technol. 23, 015019. https://doi.org/10.1088/0963-0252/23/1/015019.

Magureanu, M., Bilea, F., Bradu, C., Hong, D., 2021. A review on non-thermal plasma treatment of water contaminated with antibiotics. J. Hazard Mater. 417, 125481. https://doi.org/10.1016/J.JHAZMAT.2021.125481.

Magureanu, M., Piroi, D., Mandache, B., David, V., Medvedovici, A., Parvulescu, V.I., 2010. Degradation of pharmaceutical compound pentoxifylline in water by non-thermal plasma treatment. Water Res. 44, 3445–3453. https://doi.org/10.1016/j.watres.2010.03.020.

Magureanu, M., Piroi, D., Mandache, N.B., Parvulescu, V., 2008. Decomposition of methylene blue in water using a dielectric barrier discharge: optimization of the operating parameters. J. Appl. Phys. 104, 103306. https://doi.org/10.1063/1.3021452.

Malik, M.A., 2010. Water purification by plasmas: which reactors are most energy efficient? Plasma Chem. Plasma Process. 30, 21–31. https://doi.org/10.1007/s11090-009-9202-2.

Marx, C., Mühlbauer, V., Krebs, P., Kuehn, V., 2015. Environmental risk assessment of antibiotics including synergistic and antagonistic combination effects. Sci. Total Environ. 524–525, 269–279. https://doi.org/10.1016/j.scitotenv.2015.04.051.

Mededovic, S., Locke, B.R., 2007. Primary chemical reactions in pulsed electrical discharge channels in water. J. Phys. D Appl. Phys. 40, 7734–7746. https://doi.org/10.1088/0022-3727/40/24/021.

Miklos, D.B., Remy, C., Jekel, M., Linden, K.G., Drewes, J.E., Hübner, U., 2018. Evaluation of advanced oxidation processes for water and wastewater treatment – a critical review. Water Res. 139, 118–131. https://doi.org/10.1016/J.WATRES.2018.03.042.

Mok, Y.S., Jo, J.O., Whitehead, J.C., 2008. Degradation of an azo dye Orange II using a gas phase dielectric barrier discharge reactor submerged in water. Chem. Eng. J. 142, 56–64. https://doi.org/10.1016/j.cej.2007.11.012.

Nguyen, T.M., Kaushik, N., Nguyen, T.T., Choi, E.H., Nguyen, L.N., Kaushik, N.K., 2024. The outlook of flexible DBD-plasma devices: applications in food science and wound care solutions. Mater. Today Electron. 7, 100087. https://doi.org/10.1016/j.mtelec.2023.100087.

Nguyen, D. Van, Ho, P.Q., Pham, T. Van, Nguyen, T. Van, Kim, L., 2019. Treatment of surface water using cold plasma for domestic water supply. Environ. Eng. Res. 24, 412–417. https://doi.org/10.4491/EER.2018.215.

Oehmigen, K., Winter, J., Hähnel, M., Wilke, C., Brandenburg, R., Weltmann, K.D., Von Woedtke, T., 2011. Estimation of possible mechanisms of *Escherichia coli* inactivation by plasma treated sodium chloride solution. Plasma Process. Polym. 8, 904–913. https://doi.org/10.1002/PPAP.201000099.

Patinglag, L., Melling, L.M., Whitehead, K.A., Sawtell, D., Iles, A., Shaw, K.J., 2021. Non-thermal plasma-based inactivation of bacteria in water using a microfluidic reactor. Water Res. 201, 117321. https://doi.org/10.1016/j.watres.2021.117321.

Pavlovich, M.J., Chang, H.W., Sakiyama, Y., Clark, D.S., Graves, D.B., 2013. Ozone correlates with antibacterial effects from indirect air dielectric barrier discharge treatment of water. J. Phys. D Appl. Phys. 46, 145202. https://doi.org/10.1088/0022-3727/46/14/145202.

Rodriguez, E.E., Tarpeh, W.A., Wigginton, K.R., Love, N.G., 2022. Application of plasma for the removal of pharmaceuticals in synthetic urine. Environ. Sci. Water Res. Technol. 8, 523–533. https://doi.org/10.1039/D1EW00863C.

Rong, S., Sun, Y., 2014. Wetted-wall corona discharge induced degradation of sulfadiazine antibiotics in aqueous solution. J. Chem. Technol. Biotechnol. 89, 1351–1359. https://doi.org/10.1002/JCTB.4211.

Rong, S.P., Sun, Y.B., Zhao, Z.H., 2014. Degradation of sulfadiazine antibiotics by water falling film dielectric barrier discharge. Chinese Chem. Lett. 25, 187–192. https://doi.org/10.1016/J.CCLET.2013.11.003.

Rosenfeldt, E.J., Linden, K.G., Canonica, S., von Gunten, U., 2006. Comparison of the efficiency of OH radical formation during ozonation and the advanced oxidation processes O_3/H_2O_2 and UV/H_2O_2. Water Res. 40, 3695–3704. https://doi.org/10.1016/J.WATRES.2006.09.008.

Samukawa, S., Hori, M., Rauf, S., Tachibana, K., Bruggeman, P., Kroesen, G., Whitehead, J.C., Murphy, A.B., Gutsol, A.F., Starikovskaia, S., Kortshagen, U., Boeuf, J.-P., Sommerer, T.J., Kushner, M.J., Czarnetzki, U., Mason, N., 2012. The 2012 plasma roadmap. J. Phys. D Appl. Phys. 45, 253001. https://doi.org/10.1088/0022-3727/45/25/253001.

Singh, N.K., Wood, J.M., Karouia, F., Venkateswaran, K., 2018. Succession and persistence of microbial communities and antimicrobial resistance genes associated with International Space Station environmental surfaces. Microbiome 6. https://doi.org/10.1186/S40168-018-0585-2.

Staehelin, J., Holgné, J., 1982. Decomposition of ozone in water: rate of initiation by hydroxide ions and hydrogen peroxide. Environ. Sci. Technol. 16, 676–681. https://doi.org/10.1021/ES00104A009.

Stratton, G.R., Dai, F., Bellona, C.L., Holsen, T.M., Dickenson, E.R.V., Mededovic Thagard, S., 2017. Plasma-based water treatment: efficient transformation of perfluoroalkyl substances in prepared solutions and contaminated groundwater. Environ. Sci. Technol. 51, 1643–1648. https://doi.org/10.1021/acs.est.6b04215.

Tang, S., Yuan, D., Rao, Y., Zhang, J., Qu, Y., Gu, J., 2018. Evaluation of antibiotic oxytetracycline removal in water using a gas phase dielectric barrier discharge plasma. J. Environ. Manage. 226, 22–29. https://doi.org/10.1016/j.jenvman.2018.08.022.

Taylor, P.W., 2015. Impact of space flight on bacterial virulence and antibiotic susceptibility. Infect. Drug Resist. https://doi.org/10.2147/IDR.S67275.

Thompson, A.F., English, E.L., Nock, A.M., Willsey, G.G., Eckstrom, K., Cairns, B., Bavelock, M., Tighe, S.W., Foote, A., Shulman, H., Pericleous, A., Gupta, S., Kadouri, D.E., Wargo, M.J., 2020. Characterizing species interactions that contribute to biofilm formation in a multispecies model of a potable water bacterial community. Microbiology 166, 34–43. https://doi.org/10.1099/mic.0.000849.

Trojanowicz, M., Bojanowska-Czajka, A., Bartosiewicz, I., Kulisa, K., 2018. Advanced Oxidation/Reduction Processes treatment for aqueous perfluorooctanoate (PFOA) and perfluorooctanesulfonate (PFOS) – a review of recent advances. Chem. Eng. J. 336, 170–199. https://doi.org/10.1016/J.CEJ.2017.10.153.

Van Gils, C.A.J., Hofmann, S., Boekema, B.K.H.L., Brandenburg, R., Bruggeman, P.J., 2013. Mechanisms of bacterial inactivation in the liquid phase induced by a remote RF cold atmospheric pressure plasma jet. J. Phys. D Appl. Phys. 46, 175203. https://doi.org/10.1088/0022-3727/46/17/175203.

Wang, C., Qu, G., Wang, T., Deng, F., Liang, D., 2018. Removal of tetracycline antibiotics from wastewater by pulsed corona discharge plasma coupled with natural soil particles. Chem. Eng. J. 346, 159–170. https://doi.org/10.1016/J.CEJ.2018.03.149.

Weltmann, K.D., Von Woedtke, T., 2017. Plasma medicine - current state of research and medical application. Plasma Phys. Control. Fusion 59, 014031. https://doi.org/10.1088/0741-3335/59/1/014031.

Xu, L., Campos, L.C., Canales, M., Ciric, L., 2020. Drinking water biofiltration: behaviour of antibiotic resistance genes and the association with bacterial community. Water Res. 182, 115954. https://doi.org/10.1016/J.WATRES.2020.115954.

Xu, L., Campos, L.C., Li, J., Karu, K., Ciric, L., 2021. Removal of antibiotics in sand, GAC, GAC sandwich and anthracite/sand biofiltration systems. Chemosphere 275, 130004. https://doi.org/10.1016/J.CHEMOSPHERE.2021.130004.

Zea, L., Nisar, Z., Rubin, P., Cortesão, M., Luo, J., McBride, S.A., Moeller, R., Klaus, D., Müller, D., Varanasi, K.K., Muecklich, F., Stodieck, L., 2018. Design of a spaceflight biofilm experiment. Acta Astronaut. 148, 294. https://doi.org/10.1016/J.ACTAASTRO.2018.04.039.

Zeghioud, H., Nguyen-Tri, P., Khezami, L., Amrane, A., Assadi, A.A., 2020. Review on discharge Plasma for water treatment: mechanism, reactor geometries, active species and combined processes. J. Water Process Eng. 38, 101664. https://doi.org/10.1016/J.JWPE.2020.101664.

Ziuzina, D., Patil, S., Cullen, P.J., Keener, K.M., Bourke, P., 2013. Atmospheric cold plasma inactivation of *Escherichia coli* in liquid media inside a sealed package. J. Appl. Microbiol. 114, 778–787. https://doi.org/10.1111/JAM.12087.